Supplement of Atmos. Chem. Phys., 26, 13485–13503, 2026
https://doi.org/10.5194/acp-26-13485-2026-supplement

Atmospheric Chemistry and Physics
Open Access

Supplement of

Climate impact of contrail cirrus from hydrogen combustion aircraft

Susanne M. Pettersson et al.

Correspondence to: Susanne M. Pettersson (susannep@chalmers.se)

Contents

S1 Parameter settings for implementation of model developed by Kärcher et. al. (2015)

To implement and run the modified version of the model developed by [1] (subsequently referred to as modified K15) it needs to be parametrized. The chosen parameter values are listed in Table S1 below with short remarks, followed by the expressions mentioned in the remarks.

Table S1: Parameter settings needed for the K15 model and our base setting.

Parameter	Notation	Value	Unit	Comment
Water mass emission index for H_2	$EI_{\mathrm{H_2O,H_2}}$	8.96	kg (kg fuel)$^{-1}$	
Water mass emission index for jet	$EI_{\mathrm{H_2O,J}}$	1.23	kg (kg fuel)$^{-1}$	
Lubrication oil mass emission index	EI_o	2	mg (kg fuel)$^{-1}$	
Specific combustion heat H_2	$Q_{\mathrm{H_2}}$	122.8	MJ (kg fuel)$^{-1}$	
Specific combustion heat jet A1	Q_J	43.2	MJ (kg fuel)$^{-1}$	
Propulsion efficiency hydrogen	η	0.44	-	[2]
Air-to-fuel ratio at engine exit hydrogen	N_0	110	-	[2]
Temperature of exhaust at time zero hydrogen	T_0	660	K	[2]
Geometric mean radius of ambient aerosols	μ_a	15	nm	[1], [3], [4]
geometric width of ambient aerosols	σ_a	2.2	nm	[1]
Density of water	ρ_w	999.8	kg m^{-3}	Used for estimation of Kelvin radius in r_{act}, at 273 K
Surface tension of water	$\sigma_{s/a}$	0.0723	J m^{-2}	[5], used for estimation of Kelvin radius in r_{act}
Hygroscopicity parameter lubrication oil	κ_o	0.0006	-	[6]
Hygroscopicity parameter ambient aerosol	κ_a	0.5	-	[3], [1]
Ambient aerosol number concentration	n_a	1000	cm^{-3}	high concentration
Density of lubrication oil	ρ_o	925	kg m^{-3}	[7], [8] used for number emission index
Molar mass air	M_{air}	0.0290	kg mole^{-1}	
Initial plume radius	r_0	0.5	m	[9], [1], used for estimation of plume cooling rate
Turbulent diffusivity	ϵ	0.0285	-	from experimental data [1] ([10]), used for estimation of plume cooling rate
Exit speed of exhaust	u_0	400	m s^{-1}	[1], used for estimation of plume cooling rate
Dilution parameter	β	0.9	-	[11], used for estimation of plume cooling rate

S1.1 Kelvin radius

The Kelvin radius is calculated according to:

$$r_k = \frac{4\sigma_{s/a} M_{water}}{R_M T \rho_w} \tag{S1}$$

where, M_{water} is the molar mass of water (18.01528×10^{-3} kg Mole^{-1}) and R_M the universal molar gas constant (8.314463 J (Mole K)$^{-1}$). We have used a constant value of the Kelvin radius (r_k), fixing the temperature in the above expression to $T = 273K$ and corresponding density of water to $\rho_w = 999.8$ kg m^{-3}. This gives $r_k \approx 2.30 \times 10^{-9}$. In [1] the Kelvin radius is set to 1 nm and in [5] it is set to the expression according to Eq. (S1) with $T = 298.15$K. We chose a fixed value of the Kelvin radius as in K15 for simpler implementation. At our chosen temperature of $T = 273$K water droplet formation takes place in the plume as it is cooling to ambient conditions.

S1.2 Plume cooling rate

The equation for plume cooling rate mentioned in Table S1 can be found in [1] Eq. (10) and (14).

S1.3 Number emission index

We calculate the number emission index for lubrication oil as in Eq. (7) in [1]

$$EI_{\text{n,oil}} = \frac{3EI_o}{4\pi\rho_o\mu_o^3} e^{-(9/2)\text{Ln}^2\sigma_o} \tag{S2}$$

where μ_o is the median of the lubrication oil lognormal size distribution and σ_o the geometric width.

S1.4 Further assumptions:

Ambient aerosol size distribution and properties are chosen in line with the literature for similar models ([1], [3], [4]). Ambient aerosols come in a large span of sizes, hygroscopicities and ambient concentrations. We model ambient aerosols as a single mode lognormal size distribution with a relatively large geometric width to account for the large variation in ambient aerosols. In addition, we choose a relatively high hygroscopicity parameter value of $\kappa_a = 0.5$ in order not to underestimate the contributions of ambient aerosols to ice particle formation. The ambient particle number concentration is assumed to be 1000 cm^{-3} [3].

Other assumptions needed to implement the K15 model and which approximations we have used are found in Table S3 (all other formulas needed found in [1])

Table S2: Relations needed for implementation of K15 and which approximations we have used.

Phenomenon	Notation	Name	Reference
Saturation water vapour pressure	$e_w(T)$	Goff - Gratch approximation	[12, 13]
Mean thermal speed of water molecules	$v(T)$	Maxwell-Boltzmann	
Molar volume of supercooled water	$M_\nu(T)$	-	
Latent heat evaporation	$L_w(T)$	-	[14]

S2 Activation radius correction

We added a factor to the expression for "dry" activation radius in Kärcher et. al. [1] to account for the worse fit for small κ-values like that of lubrication oil,

$$r_{act} = s^{-2/3}\frac{r_k}{(54\kappa)^{1/3}} \quad \rightarrow \quad \alpha_0\kappa^{\alpha_1}s^{-2/3}\frac{r_k}{(54\kappa)^{1/3}}, \tag{S3}$$

where r_k is the Kelvin radius from Eq. (S1). The functional form $\alpha_0\kappa^{\alpha_1}$ was found by visual inspection from corrections to improve the approximation to the actual relation which is at the local maximum (critical saturation ratio) of the Kappa-Köhler equation

$$S(r) = \frac{r^3 - r_d^3}{r^3 - r_d^3(1-\kappa)}\exp\left(\frac{4\sigma_{s/a}M_w}{RT\rho_w r}\right). \tag{S4}$$

The local maxima for varying dry radii, r_d, was found using Wolfram Mathematicas FindMaxima function. With the functional form the parameters $\alpha_0 = 1.16788$ and $\alpha_1 = 0.186086$ where then found with Wolfram Mathematica function FindFit which uses a least squares solution. The fit was calibrated such that the $\alpha_0\kappa^{\alpha_1} \approx 1$ at $\kappa = 0.5$ since no correction is needed for larger values of κ. Fig. S1 below shows our fit compared to the original approximation in Eq. (S3) and the critical saturation ratio found from the κ-Köhler equation S4.

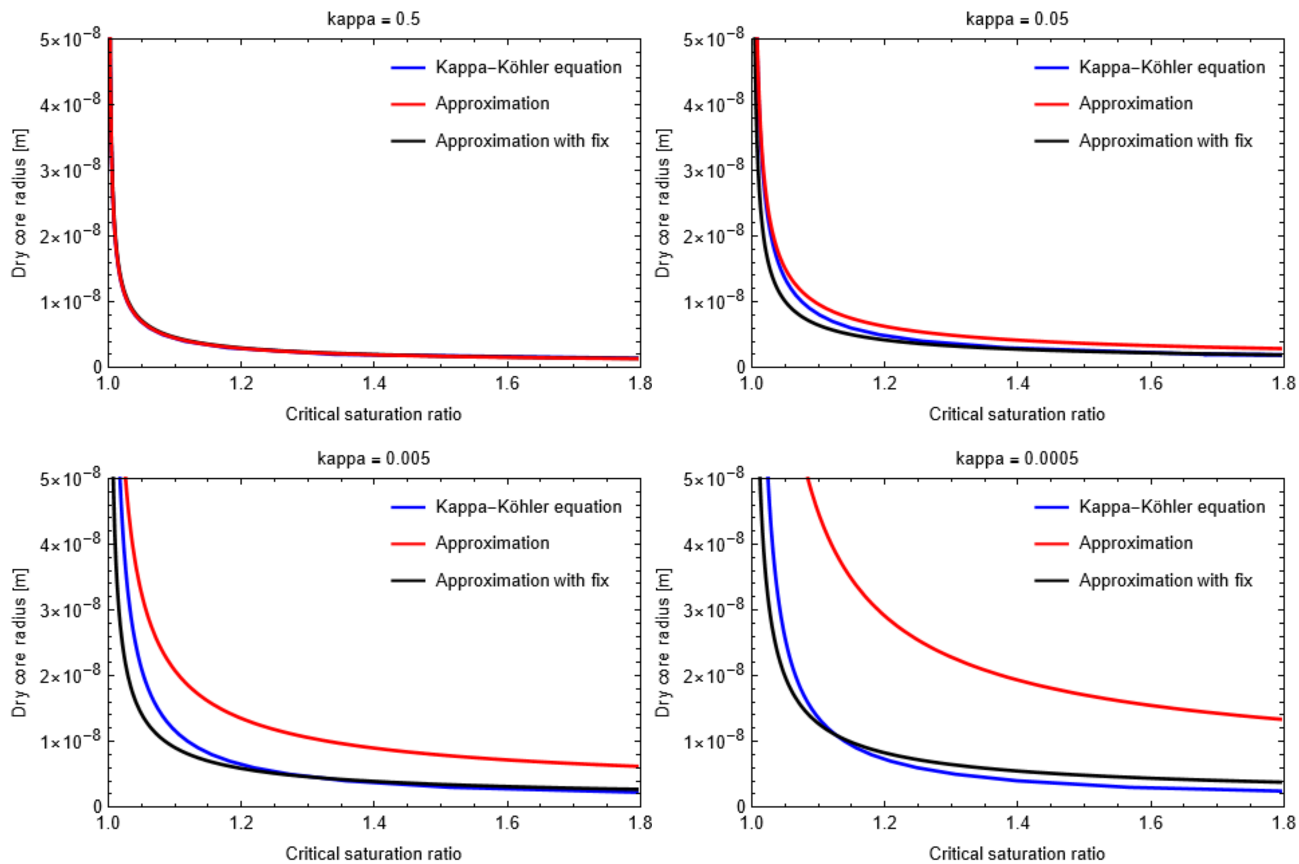

Figure S1: Illustration of how well our approximate fit (black line) and the approximate fit by [1] (red line) captures the relationship between dry core radius and critical supersaturation calculated with the Kappa-Köhler equation (blue line).

S3 Activation emulators

In this study we make use of the K15 model [1] modified as described in Sec. S2, in order to estimate the number of formed ice particles N_{ice} in the jet phase of the contrail for different ambient conditions and aircraft exhaust parameters. The amount of activated ice particles is used as input to the Contrail Cirrus Prediction model (CoCiP) [15] which then simulates the evolution of the contrail/contrail cirrus and calculates its energy forcing (EF) if the contrail is persistent. In order to reduce the run time for the combined modified K15 model and CoCiP we do not run the full modified K15 model when running CoCiP but rather an emulator, or activation function, for ice particles based on the modified K15.

The particles available for contrail formation for hydrogen combustion are limited to ambient aerosols that get entrained into the expanding plume and to emitted lubrication oil particles. For ambient aerosols we chose to generate activation rates for lognormal particle size distributions with geometric mean radius and geometric width $\mu_a = 15$ nm, $\sigma_a = 2.2$ respectively and a hygroscopicity set to $\kappa_a = 0.5$. As outlined in the main text the particle size distribution and hygroscopicity of lubrication oil are highly uncertain. Because of the large variations and uncertainties we included a range of values for the geometric mean radius and geometric width of the particle size distribution μ_o = 5-25 nm and $\sigma_o = e^{0.25}$ to $e^1 \approx$ 1.28-2.72 in our emulator of lubrication oil activation. The hygroscopicity we kept at the value $\kappa_o = 6 \times 10^{-4}$ regarding this as an upper limit in line with [6] and the mass droplet emission index EI_o = 2 mg (kg fuel)$^{-1}$ when finding the functional form of the emulator. However, we separately test the sensitivity of these assumptions. We generated data over a large span of ambient conditions T_a = 180-250 K, p_a = 100-600 hPa, rh = 0.1-1 to be sure to capture all relevant ambient conditions for contrail formation.

The activation of a species of particles l is according to K15 Eq. (40)

$$\begin{aligned} \phi_l &\approx \frac{1}{1 + (r_{act,l}/\mu_{r_l})^{\zeta_l}} \\ \zeta_l &= \frac{4}{\sqrt{2\pi}\ln\sigma_l}. \end{aligned} \tag{S5}$$

These expressions are derived in Appendix A in K15. If there are more particle species than one then the activation radius and slope parameter ζ are given by number weighted averages

$$\begin{aligned} \zeta &= \sum_l \phi_l n_{wl}\zeta_l / \sum_l \phi_l n_{wl} \\ r_{act} &= \sum_l \phi_l n_{wl} r_{act,l} / \sum_l \phi_l n_{wl}. \end{aligned} \tag{S6}$$

The expression for the total water droplet number concentration for lubrication oil and ambient aerosols is given by

$$n_w = \phi_o n_{wo} + \phi_a n_{wa}. \tag{S7}$$

n_{wa} is the number concentration of ambient aerosols in the plume which is given by what we call the entrainment factor and the number concentration of ambient aerosols $n_{wa} = E_a n_a$. The ice particle number we get from K15 at the time of quenching of the supersaturation forcing as outlined in the main text and well explained in [1]. We make emulators of ϕ from Eq. (S5) for both lubrication oil and ambient aerosols and in addition the entrainment factor for aerosols at the time of quenching when both are included in the model.

S3.1 Lubrication oil activation emulator

The activation function for lubrication oil A_o is a function of particle size distribution (μ_o, σ_o), ambient temperature T_a, ambient pressure p_a, relative humidity rh, and the critical temperature for fulfilling SAC for contrail formation T_{crit}. The critical temperature in turn is a function of the ambient pressure. The functional form was found manually by visual inspection and appreciation of known trends, for example, for oil particle geometric mean radius μ_o = 5 nm the activation decreases due to the Kelvin effect. Once a functional form capturing the main features was found parameters were fitted using least squares fit. The emulator for lubrication oil is given below

$$\begin{aligned} &A_o(\mu_o, \sigma_o, T_a, rh, p_a, T_c(p_a)) = \\ &1 - \frac{a}{b(\sigma_o)c(Ta, T_c)} \times \left(1 - \frac{d}{1 + e^{-2f(\mu_o,\sigma_o,rh,p_a)g(T_a,rh,T_c)}}\right) \\ &- h(\mu_o, \sigma_o, p_a) - i(\mu_o, \sigma_o, p_a) \end{aligned} \tag{S8}$$

$$
\begin{aligned}
&b(\sigma_o) = 1 + e^{-2b_1(\ln(\sigma_o)-b_2)} \\
&c(T_a, T_c(p_a)) = 1 + e^{-2c_1(T_a - T_c(p_a))} \\
&f(\mu_o, \sigma_o, rh, p_a) = \frac{f_1 \mu_o^2 (1 - f_2 rh^4)}{(1 + f_3(\sigma_o, p_a))} \\
&f_3(\sigma_o, p_a) = \frac{p_a - 1}{1 + e^{-2f_{31}(\ln(\sigma_o)-f_{32})}} \\
&g(T_a, rh, T_c(p_a)) = T_a - T_c(p_a) + g_1 + g_2 rh^5 \\
&h(\mu_o, \sigma_o, p_a) = h_1(\mu_o) h_2(\sigma_o) h_3(p_a) \\
&h_1(\mu_o) = 1 - \frac{1}{1 + e^{-2h_{11}(\mu_o - h_{12})}} \\
&h_2(\sigma_o) = \frac{1}{1 + e^{-2h_{21}(\ln(\sigma_o)-h_{22})}} \\
&h_3(p_a) = \frac{1}{1 + e^{-2h_{31}(p_a - h_{32})}} \\
&i(\mu_o, \sigma_o, p_a) = i_1 i_2(\mu_o) i_3(\sigma_o) i_4(p_a) \\
&i_2(\mu_o) = 1 - \frac{1}{1 + e^{-2i_{21}(\mu_o - i_{22})}} \\
&i_3(\sigma_o) = i_{31} - \frac{1}{1 + e^{-2i_{32}(\ln(\sigma_o)-i_{33})}} \\
&i_4(p_a) = \frac{1}{1 + e^{-2i_{41}(p_a - i_{42})}}
\end{aligned}
\tag{S9}
$$

With parameter values

$$
\begin{aligned}
&a = 1.40049540e-01 \\
&b_1 = 7.36579929e+00, b_2 = 6.48662671e-01 \\
&c_1 = 1.51822516e-02, \\
&d = 1.40339479e+00 \\
&f_1 = 1.85507396e-03, f_2 = 3.43463012e-01 \\
&f_{31} = 5.22241740e-01, f_{32} = 6.50965671e-01 \\
&g_1 = -2.29977889e-01, g_2 = 2.06582986e+00 \\
&h_{11} = 1.97979803e-01, h_{12} = 1.00354769e+01 \\
&h_{21} = 4.53390483e+01, h_{22} = 3.70948235e-01 \\
&h_{31} = 8.31021522e-02, h_{32} = 1.32467631e+01 \\
&i_1 = 2.74061220e+01 \\
&i_{21} = 4.40588177e-01, i_{22} = 6.36974326e+00 \\
&i_{31} = 9.56418434e-01, i_{32} = 2.85824957e-01, i_{33} = -4.47149952e+00 \\
&i_{41} = 7.74184182e-01, i_{42} = 1.70779042e+00.
\end{aligned}
\tag{S10}
$$

Even though this is a large and complicated expression it is of course not in complete agreement with the underlying modified K15 model output. Especially activation at low and high air pressures ($<$ 150 hPa and $>$ 350 hPa) for small lubrication oil geometric mean radius are not as accurate as more moderate air pressures or larger geometric mean radius. However, contrail formation and persistence are not as prevalent at these ambient air pressures. Despite the different frequencies of contrail formation at different air pressures we fitted the parameters with equal weight to all air pressures (and relative humidities). This might mean a slightly better fit at these pressures at the expense of a slight reduction in accuracy at moderate air pressures, but also reduces the amount of arbitrary choices in weighting air pressures in the fitting. In Fig. S2 and Fig. S3 examples of our lubrication oil activation emulator and results from the modified K15 are shown for all geometric mean radius and geometric widths at $rh = 70\%$ and $p_a = 250$ hPa and the entire span of pressures and relative humidities for $\mu_o = 5$ nm and $\sigma_o = e^{0.25}$ respectively.

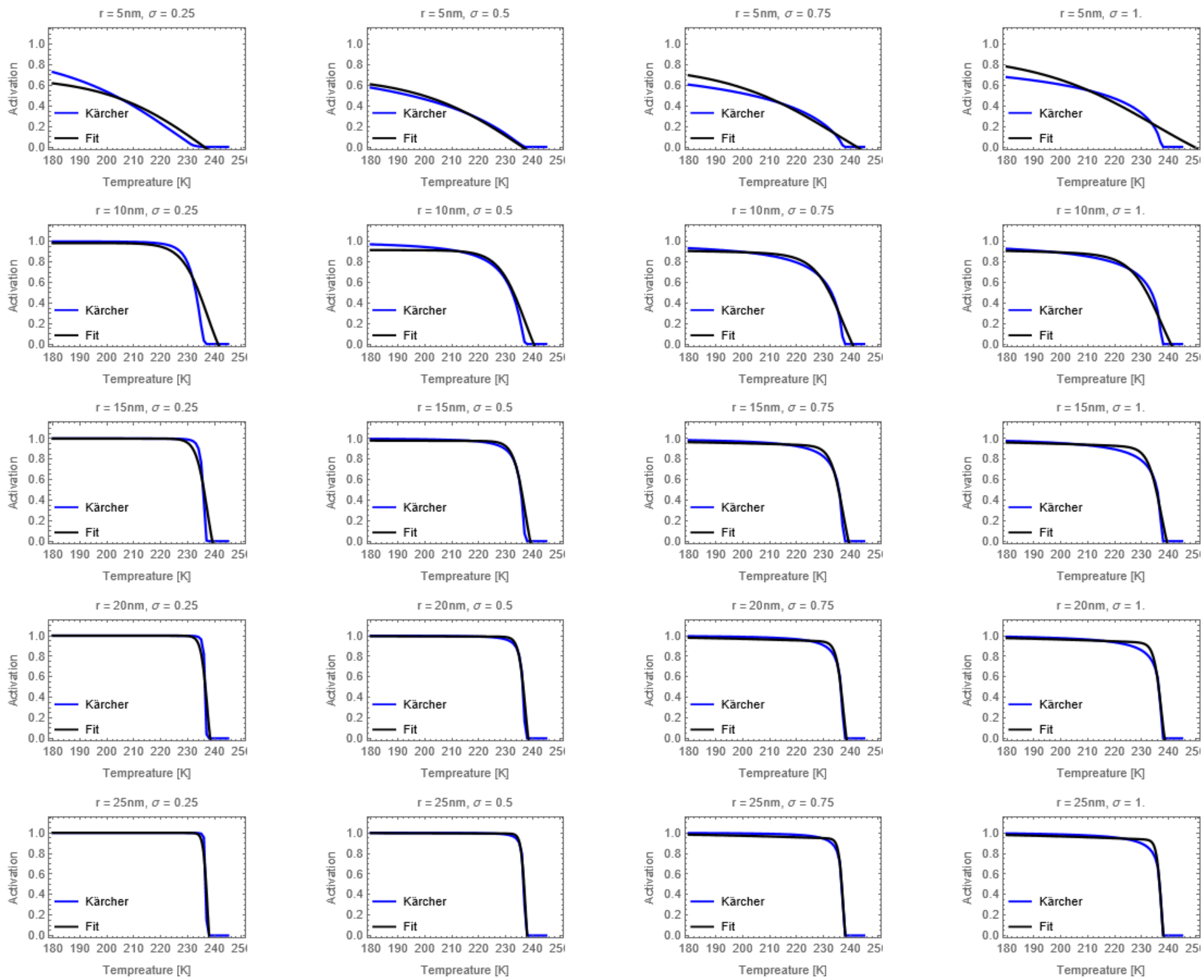

Figure S2: The figure shows examples of how the activation emulator emulates the output from the K15 model for lubrication oil particles over a range of different geometric mean radius and geometric widths at $rh = 70\%$ and $p_a = 250$ hPa.

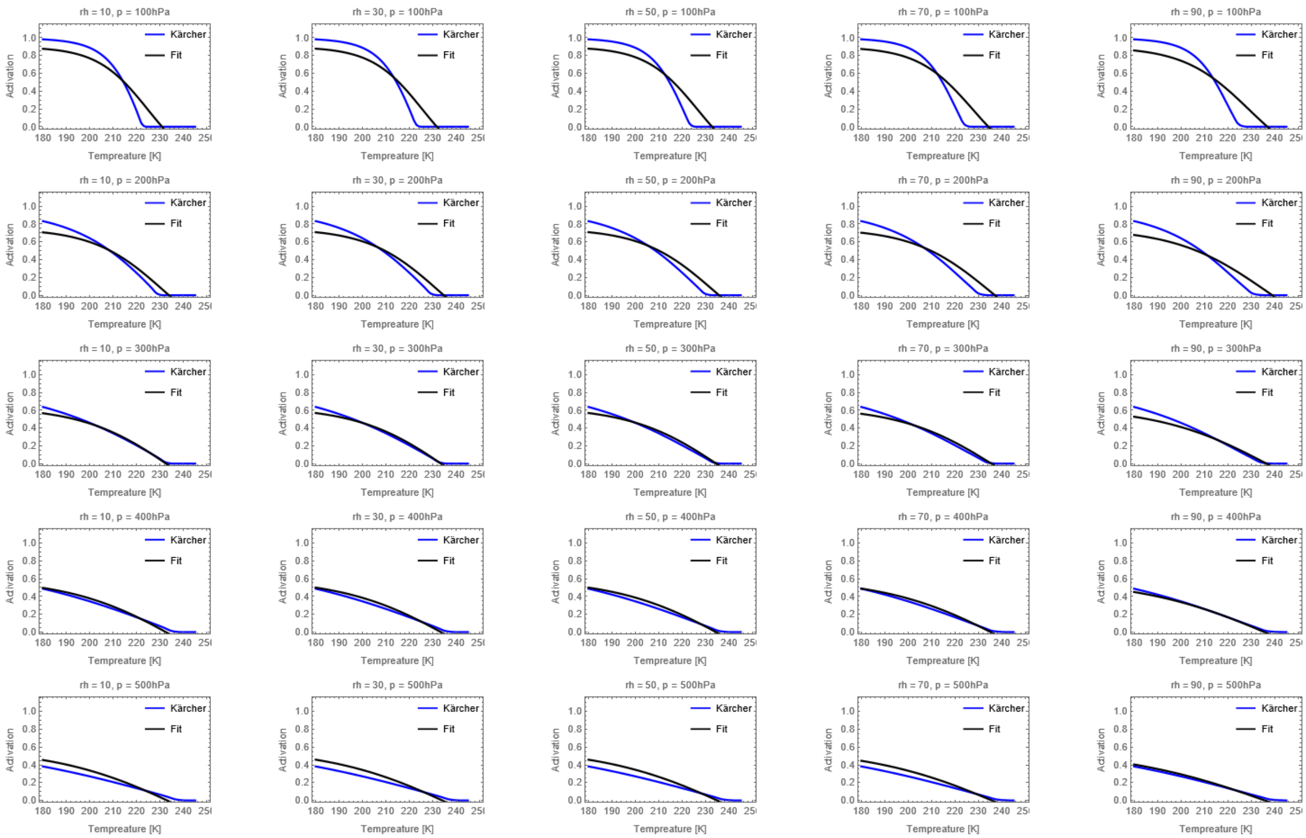

Figure S3: The figure shows examples of how the activation emulator emulates the output from the K15 model for lubrication oil particles for different relatives humidities and pressures for $\mu_o = 5$ nm and $\sigma = e^{0.25}$.

The activation obtained for lubrication oil from the modified K15 depends on the choice of κ_o and EI_o. We chose not to include these variables in our emulator, in order to keep the functional complexity down. However, the functional form was flexible enough to capture the cases of our sensitivity analysis using $\kappa_o = 0.1$ and $\mathrm{EI}_o = 20$ mg (kg fuel)$^{-1}$ with different sets of fitted parameters obtained by a least squares approach. The reason for this is that both these cases of the sensitivity analysis lead to higher activation of the lubrication oil, which are easier to emulate. Below are the parameter settings for the two sensitivity analysis cases $\kappa_o = 0.1$:

$$
\begin{aligned}
&a = 1.83272884e-01\\
&b_1 = 4.30205937e+00, b_2 = 7.13619714e-01\\
&c_1 = 3.92789497e-02,\\
&d = 1.52163826e+00\\
&f_1 = 6.30052888e-03, f_2 = 5.88546882e-01\\
&f_{31} = 3.78696793e-03, f_{32} = 9.52499644e+01\\
&g_1 = -2.77310088e-01, g_2 = 7.80894644e-01\\
&h_{11} = 2.03884382e-01, h_{12} = 2.44892848e+00\\
&h_{21} = 3.25891968e+00, h_{22} = 4.26092728e-01\\
&h_{31} = 4.59877098e-01, h_{32} = 2.03479646e+00\\
&i_1 = 5.57658123e-01\\
&i_{21} = 4.40588177e-01, i_{22} = 4.88921609e+00\\
&i_{31} = 6.35705412e-01, i_{32} = 4.55142297e+00, i_{33} = 6.52112505e-01\\
&i_{41} = 6.75310255e-01, i_{42} = 3.26501727e+00.
\end{aligned}
\tag{S11}
$$

$\mathrm{EI}_o = 20$ mg (kg fuel)$^{-1}$:

$$
\begin{aligned}
&a = 1.13191354e-01\\
&b_1 = 9.27653785e+00, b_2 = 6.23384277e-01\\
&c_1 = 6.56666768e-03,\\
&d = 1.32921536e+00\\
&f_1 = 1.30309620e-03, f_2 = 2.70677254e-01\\
&f_{31} = 2.27966755e-01, f_{32} = 2.91199176e-01\\
&g_1 = -6.01952951e-01, g_2 = 2.75490167e+00\\
&h_{11} = 2.34647173e-01, h_{12} = 1.32130555e+01\\
&h_{21} = 4.92386286e+01, h_{22} = 3.70439130e-01\\
&h_{31} = 8.88817482e-02, h_{32} = 1.42979324e+01\\
&i_1 = 2.02849846e+01\\
&i_{21} = 3.72701126e-01, i_{22} = 7.16631689e+00\\
&i_{31} = 9.51619794e-01, i_{32} = 2.83584916e-01, i_{33} = -4.18661787e+00\\
&i_{41} = 8.69030178e-01, i_{42} = 1.05224846e+00.
\end{aligned}
\tag{S12}
$$

S3.2 Ambient aerosol activation emulator

The activation fraction for ambient aerosols at quench is a function of ambient temperature T_a, pressure p_a, relative humidity rh, and the critical temperature for fulfilling SAC for contrail formation T_{crit} and given by

$$\phi_{em,a}(T_a, rh, T_c(p_a)) = j_1\left(1 - \frac{1}{1 + e^{-2(j_2 - rh)(T_a - T_c(p_a))}}\right), \tag{S13}$$

with parameter values $j_1 = 0.98621099$, $j_2 = 1.27258155$. Our activation emulator includes not only the fraction of activated ambient aerosols but also the fraction of the ambient aerosol concentration that gets entrained. In K15 the entrainment is calculated according to their Eq. (37)

$$\begin{aligned} E_a &= \frac{T_a}{T}(1 - D) \\ D &= \frac{T - T_a}{T_0 - T_a}, \end{aligned} \tag{S14}$$

Where T_0 is the temperature at exhaust. Since the temperature of the plume at quench is unknown we make a fit to the entrainment E_a obtained from the modified K15 model at quench. Our fit is given by

$$E_a(\mu_o, T_a, p_a) = k_1(T_a - k_2)^4 - k_3(p_a/10000) + k_4(\mu_o \times 10^9 - k_5) + k_6 \tag{S15}$$

with parameter values $k_1 = 1.61453153e-10$, $k_2 = 5.76886132e-01$, $k_3 = 3.41028865e-02$, $k_4 = 1.30248424e-03$, $k_5 = 9.72503036e+00$ and $k_6 = 5.19101870e-01$. Here we actually have a slight dependence of the lubrication oil geometric mean radius. Our activation emulator for ambient aerosols (including both entrainment and activation) is then given by

$$A_a = E_a\phi_{em,a} \tag{S16}$$

and shown for all geometric mean radius and geometric widths of lubrication oil at $rh = 70\%$ and $p_a = 250$ hPa in Fig. S4.

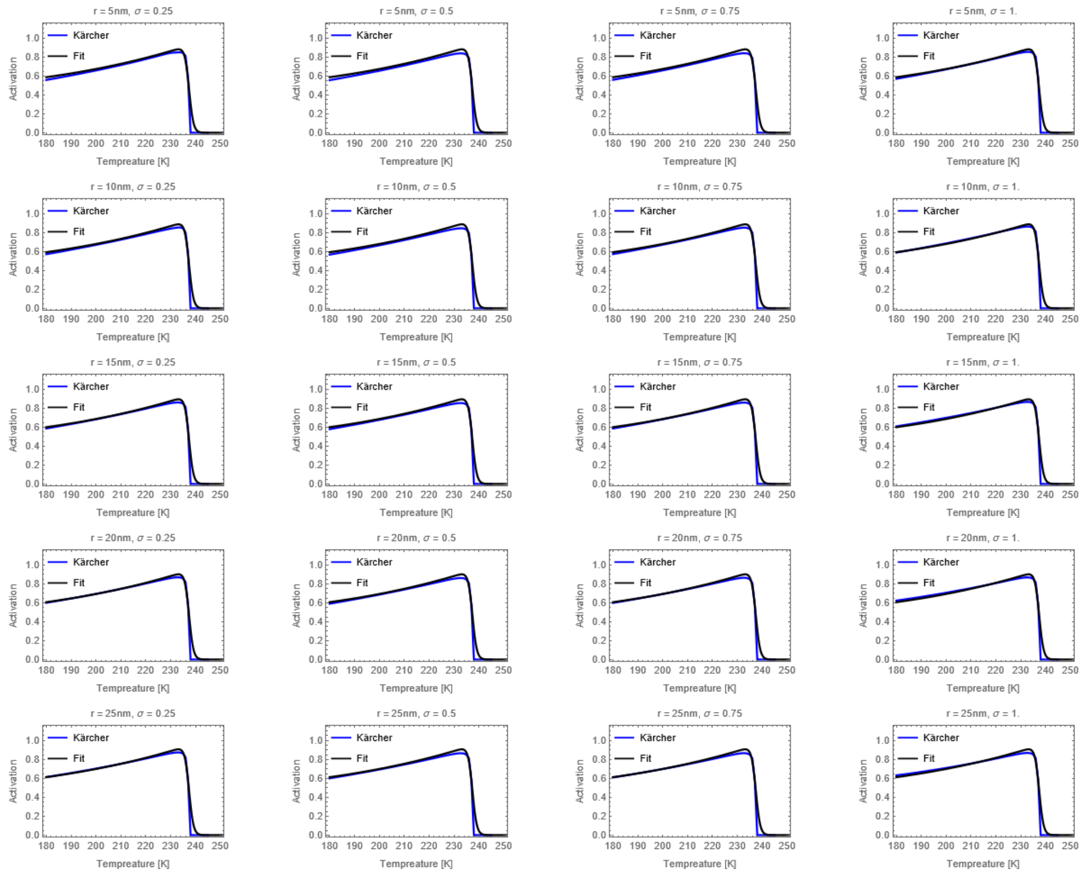

Figure S4: The figure shows examples of how the activation emulator emulates the output from the K15 model for ambient aerosols for different assumptions on lubrication oil size distributions covering a range of different geometric mean radius and geometric widths at $rh = 70\%$ and $p_a = 250$ hPa

S4 Implementation in CoCiP

To approximate the amount of formed ice particles from soot particles the original version of CoCiP uses an activation function based on raw data from [16]

$$A_s(T_a, T_{crit}) = \max(-0.661e^{(T_a - T_c(p_a))} + 1.0, 0). \tag{S17}$$

From the activated soot number emission index, $n_{\mathrm{act,s}} = A_s EI_{\mathrm{n,s}}$ (kg fuel)$^{-1}$, CoCiP calculates the number of activated soot particles per meter flight according to $N_s = n_{\mathrm{act,s}} \times ff/v_{\mathrm{tas}}$ with the fuel flow ff and true airspeed v_{tas} of the aircraft. This same procedure is used for lubrication oil since we can calculate a lubrication oil number emission index from the mass emission index and Eq. (S2) where a lognormal distribution is assumed [1].

Using the emulators based on the modified K15 model, one gets the activation of both lubrication oil and entrained ambient aerosols. Number of ice particles per meter flight formed from lubrication oil particles is calculated according to

$$N_o = EI_{n,o} \times A_o \times ff/v_{\mathrm{tas}}. \tag{S18}$$

To get the amount of ice particles per meter flight formed from ambient aerosols we use the expression

$$N_a = E_a \times A_a \times n_a \times n_{\text{engine}} \times A_{\text{plume}}, \tag{S19}$$

where A_{plume} is the cross sectional area of the plume and n_{engine} is the number of engines. For the area of the plume at quench we use a fitted function $A_{\text{plume}}(T_a) = 2 \times 10^{-6}(T_a - 180)^4 + 5$ which is fitted to the area at time of quench from the K15 model. The sum of N_o and N_a gives the number of ice particles formed in the jet phase. CoCiPs internal calculation of ice particle loss in downwash f_{surv} is subsequently applied.

S5 Random dates used in sensitivity analysis

Table S3: Twenty randomly selected dates from the year 2019 used in sensitivity analysis simulations.

Month	Days
January	23
February	-
March	22
April	16
May	11
June	3, 13, 26
July	21
August	10, 18, 29
September	9, 19, 27
October	5, 15
November	1
December	18, 20, 25

S6 Quantification of activation emulator error propagation to end results

To quantify the difference in the final results (average energy forcing per flight meter from CoCiP) between our emulators and the modified K15 model we implemented the modified K15 directly in CoCiP for a smaller number of cases using the base case settings, being EUR = 1, $\text{EI}_o = 2$ mg (kg fuel)$^{-1}$, and $\kappa_o = 6 \times 10^{-4}$ and ambient aerosol concentration $n_a = 1000cm^{-3}$. Because of run-time constraints we chose 30 random gridpoints in the same coordinate span and random dates as in our sensitivity analysis in the main paper, i.e. latitude [-70, 70], longitude [-180,180] and the dates from S5 and simulated contrails for the levels $p_a = 200, 225, 250, 300$ hPa. This resulted in 8586 contrails analysed, with representative statistics of meteorological conditions and ranging from $T_{a,max} = 241.16374$, $T_{a,min} = 194.99529$, $rhi_{max} = 1.7$, $rhi_{min} = 0.2243631$.

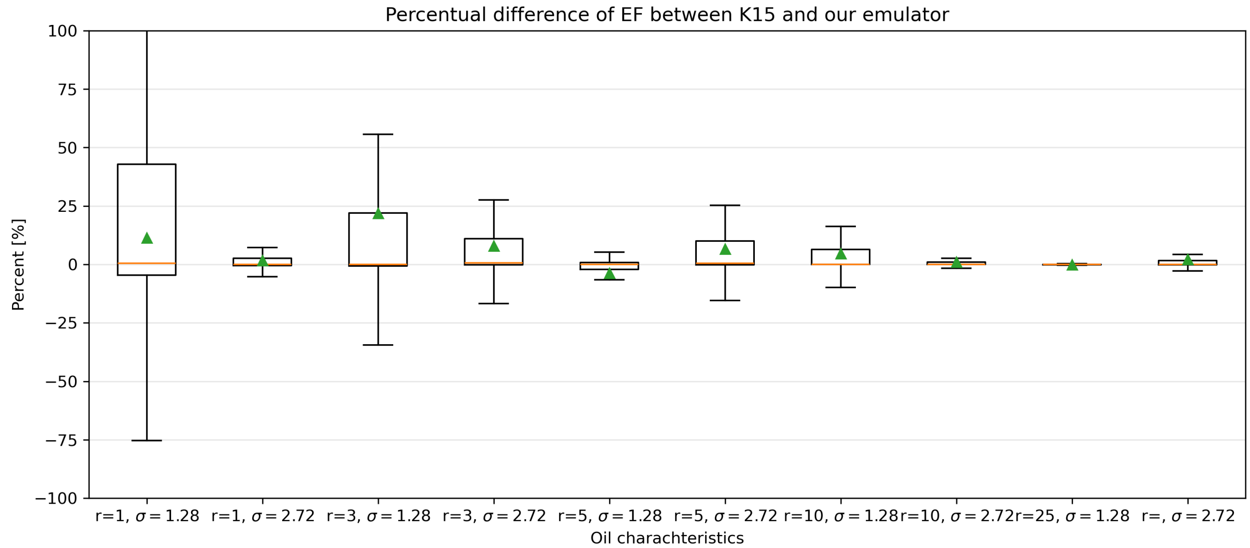

Figure S5: Box and whiskers plot of error statistics. The percentages are calculated according to $\mathrm{EFpfm}_{K15} - \mathrm{EFpfm}_{em})/\overline{\mathrm{EFpfm}_{K15}}$ for each generated contrail for all combinations of geometric mean radius $\mu_r = 3, 5, 10$ nm and geometric width $\sigma_r = 1.28, 2.72$. Boxes show the IQR (Inter Quartile Range), Whiskers 1.5IQR, green triangles show the mean and yellow line the median.

As can be seen the inter quartile range (IQR) for the error percentages are quite large for some of the oil particle size distributions. Especially for geometric mean radius $\mu_r = 3$ nm and $\sigma_r = 1.28$. The large deviations between the emulator and using the the numerical implementation of the modified K15 stem from cases where either the emulator or the modified K15 predicts activated water droplets and the other does not, which implies that one model generate an EFpfm=0 or close to zero, while the other implementation does not. The spread is to be expected to some degree, as can be seen from Fig. S2 the emulator overestimates in some cases and underestimates in some. However, the median as can be seen is close to zero and differences in the average EFpfm are 11%, 2%, 22%, 8%, -4%, 7%, 5%, 1%, -0.2% and 2% in the same order as shown in Fig. S5.

In Fig. S5 we show the EFpfm, lifetime, optical depth, mean lifetime ice number and mean lifetime radius for the six oil particle size distributions obtained with the emulator vs the numerical implementation of the modified K15 model. Hence, as can be seen in Fig. S5, the averaged output based on the emulator replicates the average output based on the numerical solution of the modified K15 very well.

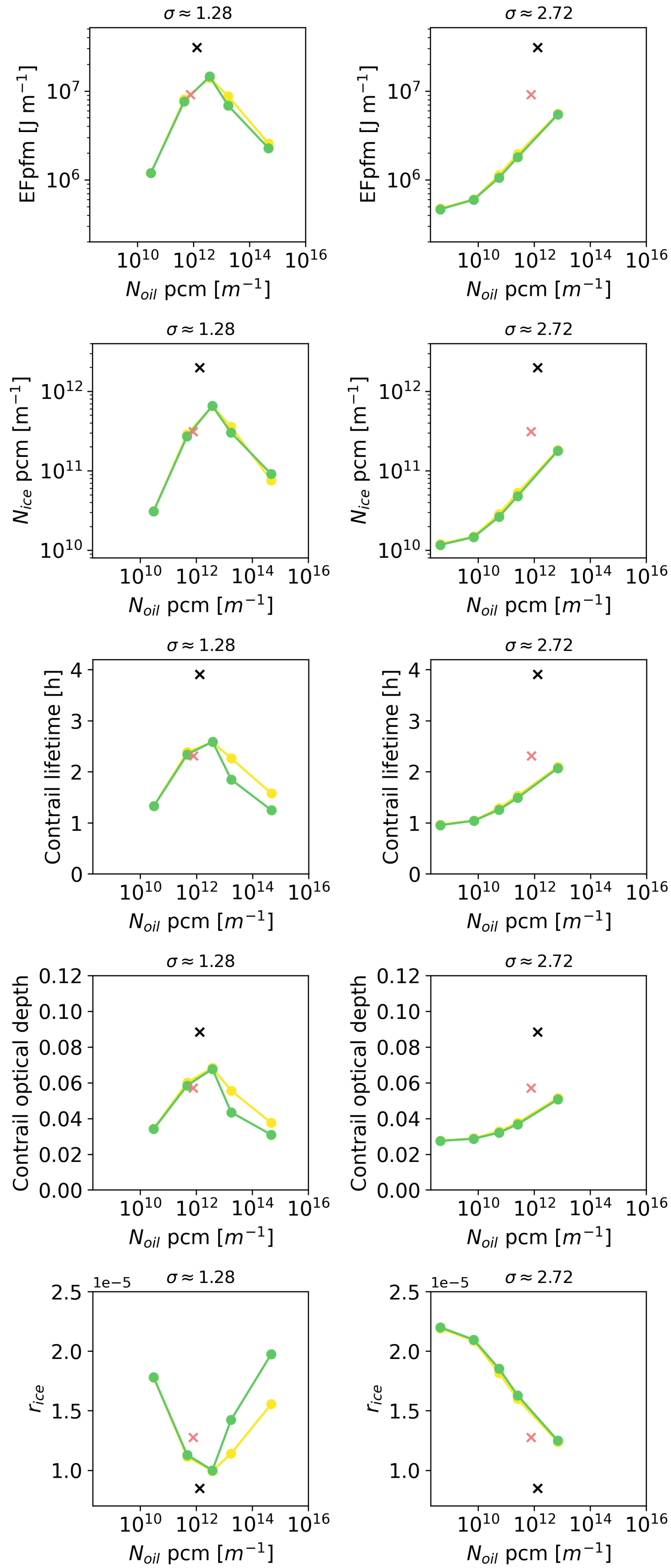

Figure S6: Figures show the CoCiP output using the modified K15 model in yellow and our emulator in green with the percentage difference in the average EFpfm as error bars. The Black marker shows the values for runs with jet A-1 fuel and pink marker our base case using our emulator in CoCiP for reference.

S7 Comparison of soot activation between K15 and CoCiP

A consistent approach to obtain ice particle numbers for soot when running CoCiP for fossil jet fuel would be to use an emulator of the modified K15 model also for that. We chose instead to use CoCiPs own activation function for soot because of the close similarity in activation (from soot to ice) between the two approaches and simplicity in implementation. CoCiP activates soot particles to ice particles according to Eq. (S17). Activation of soot particles from the modified K15 model can be seen in Fig. S7 and CoCiP activation from Eq. (S17) in Fig. S8 for ambient relative humidities in the span 20-100%, ambient pressures in the span 100-500 hPa and varying ambient temperatures.

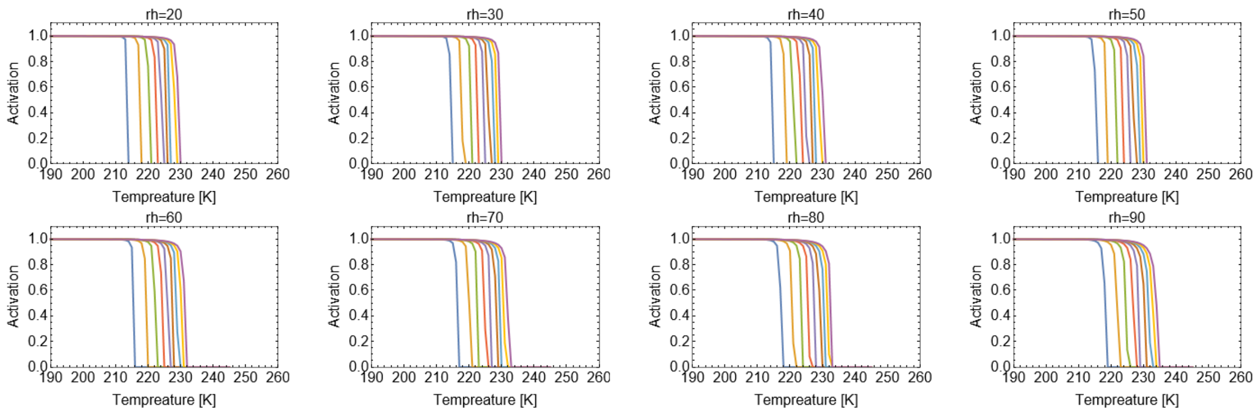

Figure S7: Activation of soot from the K15 model. The different plots show activation of soot for different relative humidities. The different curves in the plot represents different ambient pressures, the blue curve representing the lowest pressure 100 hPa followed by successively higher pressures up to 500 hPa.

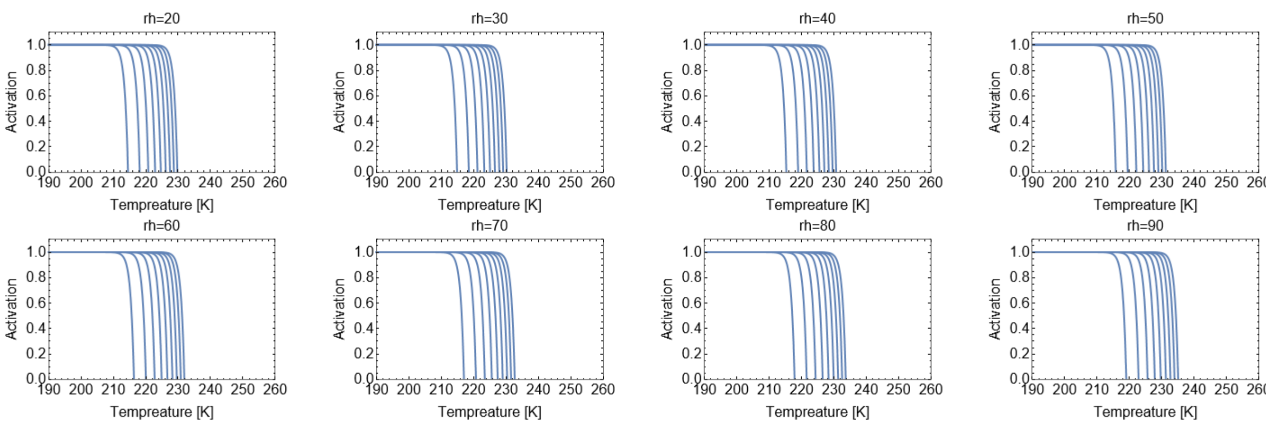

Figure S8: Activation of soot in CoCiP. The different plots show activation of soot for different relative humidities. The different curves in the plot represents different ambient pressures.

For further comparison on the energy forcing output obtained with either approach we implemented the modified K15 directly in CoCiP for soot activation. For implementation of the modified K15 we used the values for soot as in [1] $\mu_{r,s} = 25nm$ and $\sigma_{r,s} = 1.65$, $\kappa_s = 0.005$ and $EI_s = 40mgcm^{-3}$. We chose 60 random gridpoints in the coordinate span latitude [-70, 70], longitude [-180,180] and random dates as listed in S5 and simulated contrails for levels 200, 225, 250, 300 hPa. This resulted in 8869 contrails analysed, with representative statistics of meteorological conditions and ranging from $T_{a,max} = 228.1154$, $T_{a,min} = 192.8358$, $rhi_{max} = 1.7$, $rhi_{min} = 0.575085$.

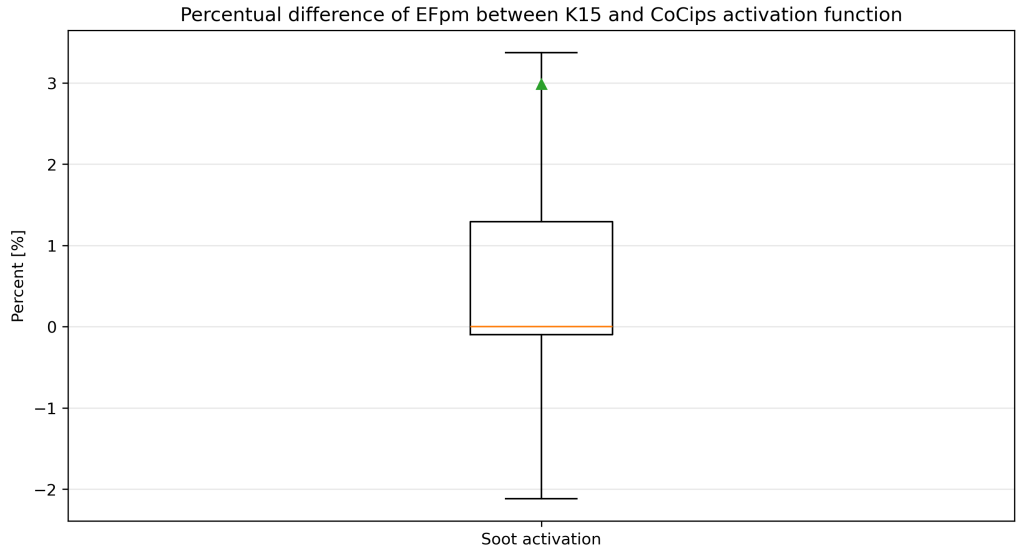

Figure S9: Box and whiskers plot of error statistics. The percentages are calculated according to $(\text{EFpfm}_{K15} - \text{EFpfm}_{CoCip})/\text{EFpfm}_{K15}$ for each generated contrail. Boxes show the IQR (Inter Quartile Range), Whiskers 1.5IQR, green triangle show the mean and yellow line the median.

S8 Sensitivity analysis to ambient aerosol concentration

Ambient aerosols are highly variable in concentration, size distribution, and composition throughout the atmosphere. Here we perform a sensitivity analysis of how average EFpfm depends on ambient aerosol number concentration by analysing the impacts of shifting the distribution an order of magnitude up and down. Other characteristics of the ambient aerosols are kept constant. In Fig. S10 we show simulations for $\mu_o = 1, 3, 5, 10, 25$ nm and for two values of geometric width $\sigma_o = 1.28, 2.72$, i.,e. the characteristics of the lubrication oil distribution, for the three cases with ambient aerosol number concentration being $n_a = 10^2, 10^3, 10^4$ cm^{-3}. In Fig. S11 we show the percentage of ice particles after downwash formed on ambient aerosols for our base case relative to total formed ice particles after downwash.

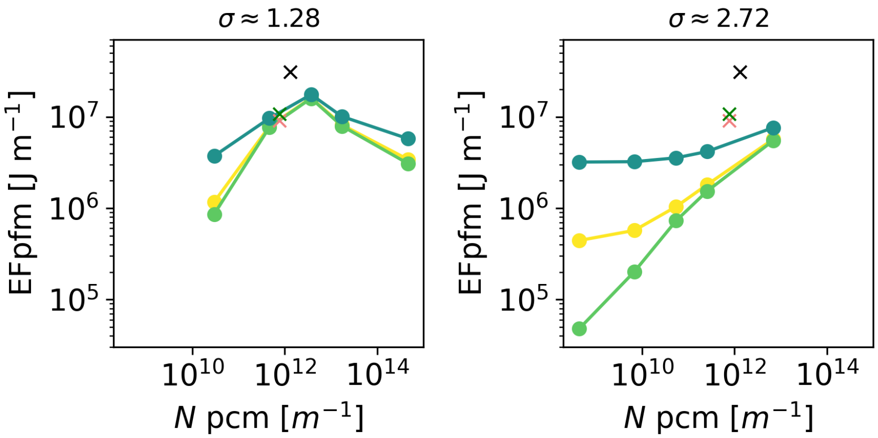

Figure S10: The plots show average EFpfm for three cases of ambient aerosol concentration $n_a = 10^2$ light green, $n_a = 10^3$ yellow and $n_a = 10^4$ dark green all else equal. All simulation are run with geometric mean radii $\mu_o = 1, 3, 5, 10, 25$nm for two geometric widths $\sigma_o = 1.28, 2.72$, for the 20 dates in S5 and with base parameter settings. The black marker show the average EFpfm for soot, pink marker for our base case and dark green for base case settings except for $n_a = 10^4\text{cm}^{-3}$.

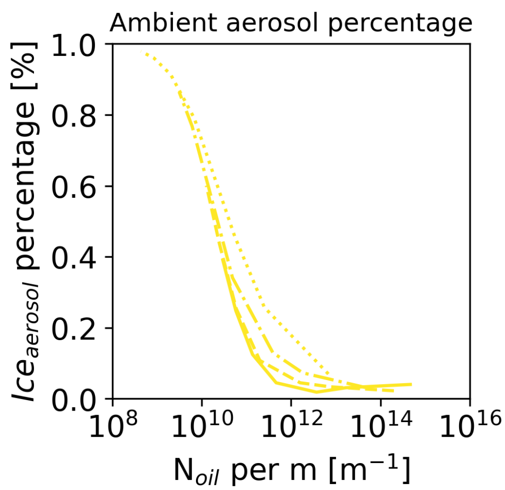

Figure S11: The plot shows percentage of ice crystals after downwash formed on ambient aerosols for all lubrication oil droplet size distributions. N_{oil} per meter is determined by the size distribution. The different lines represents the four geometric widths of the size distribution, full line $\sigma_o \approx 1.28$; stripe-dotted $\sigma_o \approx 1.65$; striped $\sigma_o \approx 2.21$; dotted $\sigma_o \approx 2.72$

As expected the change in ambient aerosol concentration has the largest impact when the lubrication of oil droplet size distribution can be described with a relatively large geometric mean radius and large geometric width (generating the smallest amount of oil droplets per meter in the exhaust N). This is in the regime where water droplet formation (and ice crystals) is dominated by ambient aerosols as seen in Fig. S11. In this regime we see a 620% increase for $n_a = 10^4\text{cm}^{-3}$ and 90% decrease for $n_a = 10^2\text{cm}^{-3}$ compared to $n_a = 10^3\text{cm}^{-3}$. In this oil droplet size distribution range the ambient aerosols dominate but lubrication oil still contributes with a few percent to total ice particle number. However, the $n_a = 10^4\text{cm}^{-3}$ case is very high number for ambient aerosol number concentration. Ambient aerosol concentrations are rarely as high and if they are tend to have smaller geometric mean radius than assumed here [17]. Still this pessimistic best case of almost no contribution from lubrication oil but high ambient aerosol concentration is a 44% reduction compared to our base case and 90% reduction compared to conventional fossil jet fuel.

References

1. Kärcher, B., Burkhardt, U., Bier, A., Bock, L. & Ford, I. The microphysical pathway to contrail formation. *Journal of Geophysical Research: Atmospheres* **120,** 7893–7927. ISSN: 2169-897X (2015).
2. Patrao, A. C., Jonsson, I., Xisto, C., Lundbladh, A. & Grönstedt, T. Compact heat exchangers for hydrogen-fueled aero engine intercooling and recuperation. *Applied Thermal Engineering* **243,** 122538. ISSN: 1359-4311 (2024).
3. Bier, A. *et al.* Contrail formation on ambient aerosol particles for aircraft with hydrogen combustion: a box model trajectory study. *Atmospheric Chemistry and Physics* **24,** 2319–2344. ISSN: 1680-7316 (2024).
4. Yu, F., Karcher, B. & Anderson, B. E. Revisiting contrail ice formation: Impact of primary soot particle sizes and contribution of volatile particles. *Environmental Science Technology.* ISSN: 0013-936X (2024).
5. Petters, M. & Kreidenweis, S. A single parameter representation of hygroscopic growth and cloud condensation nucleus activity. *Atmospheric Chemistry and Physics* **7,** 1961–1971. ISSN: 1680-7324 (2007).
6. Lambe, A. *et al.* Laboratory studies of the chemical composition and cloud condensation nuclei (CCN) activity of secondary organic aerosol (SOA) and oxidized primary organic aerosol (OPOA). *Atmospheric Chemistry and Physics* **11,** 8913–8928. ISSN: 1680-7324 (2011).
7. Yu, Z. *et al.* Characterization of lubrication oil emissions from aircraft engines. *Environmental science technology* **44,** 9530–9534. ISSN: 0013-936X (2010).
8. Ponsonby, J., King, L., Murray, B. J. & Stettler, M. E. Jet aircraft lubrication oil droplets as contrail ice-forming particles. *Atmospheric Chemistry and Physics* **24,** 2045–2058. ISSN: 1680-7316 (2024).
9. Lewellen, D. C. A large-eddy simulation study of contrail ice number formation. *Journal of the Atmospheric Sciences* **77,** 2585–2604. ISSN: 0022-4928 (2020).
10. Tollmien, W. Berechnung turbulenter ausbreitungsvorgänge. *ZAMM-Journal of Applied Mathematics and Mechanics/Zeitschrift für Angewandte Mathematik und Mechanik* **6,** 468–478. ISSN: 0044-2267 (1926).
11. Kärcher, B. Aviation-produced aerosols and contrails. *Surveys in geophysics* **20,** 113–167. ISSN: 0169-3298 (1999).
12. Goff, J. A. Saturation pressure of water on the new Kelvin temperature scale. *Transactions of the American society of heating and ventilating engineers,* 347–354 (1957).
13. Heating, A. S. o. & Engineers, V. *Transactions of the American Society of Heating and Ventilating Engineers* (The Society, 1925).
14. Murphy, D. M. & Koop, T. Review of the vapour pressures of ice and supercooled water for atmospheric applications. *Quarterly Journal of the Royal Meteorological Society: A journal of the atmospheric sciences, applied meteorology and physical oceanography* **131,** 1539–1565. ISSN: 0035-9009 (2005).
15. Schumann, U. A contrail cirrus prediction model. *Geoscientific Model Development* **5,** 543–580. ISSN: 1991-9603 (2012).
16. Bräuer, T *et al.* Airborne measurements of contrail ice properties—Dependence on temperature and humidity. *Geophysical Research Letters* **48,** e2020GL092166. ISSN: 0094-8276 (2021).

17. Minikin, A. *et al.* Aircraft observations of the upper tropospheric fine particle aerosol in the Northern and Southern Hemispheres at midlatitudes. *Geophysical Research Letters* **30.** ISSN: 0094-8276 (2003).